Earth, Planets and Space

FULL PAPER Open Access

Sporadic E layer characteristics at equatorial latitudes as observed by GNSS radio occultation measurements

Christina Arras[1*], Laysa Cristina Araújo Resende[2,3], Ankur Kepkar[1,4], Gethmini Senevirathna[4] and Jens Wickert[1,4]

Abstract

Scintillations in the signal-to-noise (SNR) profiles of GNSS radio occultation (RO) measurements at lower ionospheric altitudes are caused by compact layers of high ionization also known as sporadic E (Es) layers. It is widely accepted that Es layers are formed by the wind shear mechanism at northern and southern midlatitudes. However, approaching the equatorial regions, electric fields also control the formation and dispersal of these layers. In this paper we concentrate, in particular, on the occurrence rate and on the altitudes of Es layers appearing in a narrow band along the Earth's magnetic equator. We analyzed several million of RO profiles concerning sporadic E occurrence as well as altitude and observed a high daily, seasonal and longitudinal variability which is controlled partly by zonal winds and electric fields. Especially Es layers at higher altitudes show a clear anticorrelation with the zonal electric field intensity measured by the Swarm satellites. Further, we solve the existing contradiction of Es layer signatures being present in equatorial ionosonde measurements while they are only rarely seen in RO recordings.

Keywords: GNSS radio occultation, Sporadic E layers, Equatorial ionosphere

*Correspondence: arras@gfz-potsdam.de

[1] GFZ German Research Centre for Geosciences, Potsdam, Germany
Full list of author information is available at the end of the article

Graphical Abstract

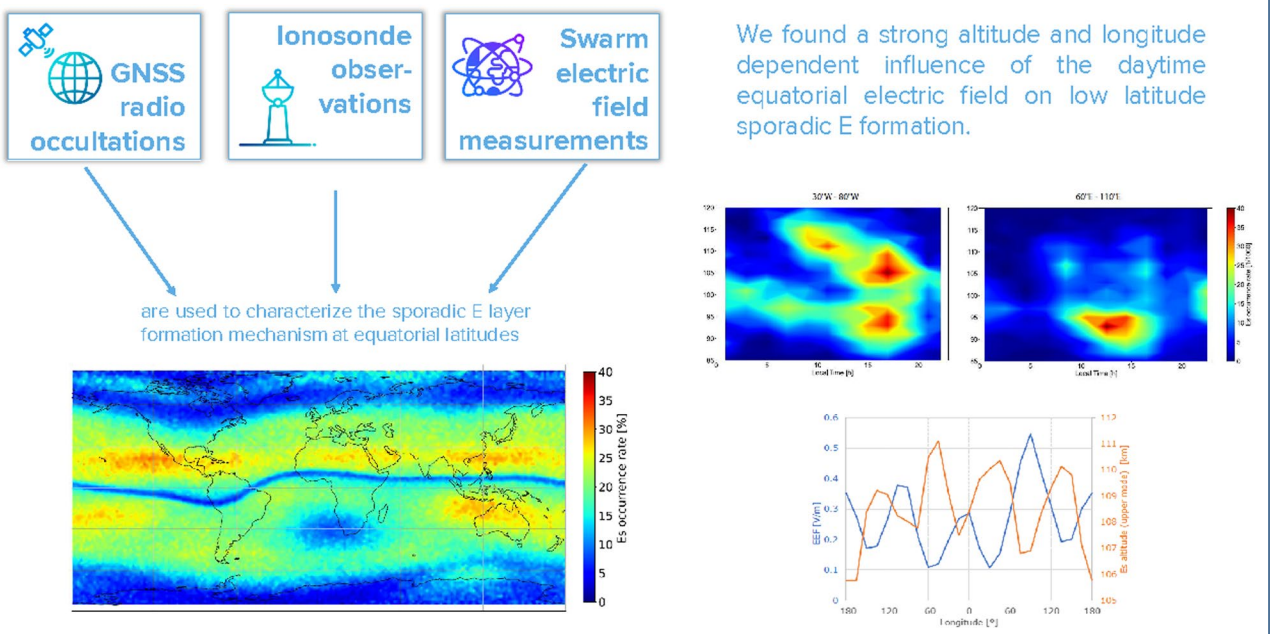

Introduction

Sporadic E layers (Es) are defined as thin electron density enhancements that commonly appear at the altitude range between 90 km and 130 km. They are most frequently observed at mid-latitude during the summer season. The Earth's lower ionosphere and in particular sporadic E layers are strongly influenced by coupling processes between the neutral atmosphere, ionosphere, and magnetosphere. It is widely accepted that Es emerges in line with windshear theory (Yamazaki et al. 2022; Whitehead 1961; Axford 1963; Haldoupis 2010; Jayachandran et al. 1999). It explains that the layers result from complex interactions of meteoroids bringing metallic ions into our atmosphere, dynamics and especially vertical shears of the zonal wind of the upper mesosphere and lower thermosphere, and Earth's magnetic field parameters (Macleod 1966; Mathews 1998; Shinagawa et al. 2017).

At low latitudes, especially close to the magnetic equator, the wind shear mechanism is not effective enough to form strong Es layers identified as the blanketing type (Esb) in ionograms. The vertical wind shear associated with the tidal winds is not efficient in the the magnetic equator's vicinity since the magnetic field's horizontal configuration does not allow the denser Es layer formation (Resende et al. 2016; Moro et al. 2016).

Along the magnetic equator flows the equatorial electrojet (EEJ) current. During daytime the electric current is directed eastward and driven by the zonal and vertical electric fields. This current occurs due to the upward vertical polarization electric field, which drives an additional Hall current superimposed to the Pedersen current around 95–115 km (Forbes 1981; Resende et al. 2021).

Ionograms from stations that are located near the magnetic equator sometimes reveal signatures of the Esq (equatorial type sporadic E) layer. This layer is characterized by a diffuse and non-blanketing Es trace in ionograms, reaching most of the frequency scale (Whitehead 1961; Knecht and McDuffie 1962; Resende et al. 2013). The most significant characteristic of the Esq layer is that it is not an enhanced ionization of the plasma as the usual sporadic E layers produced by wind shear. The Es patches are related to gradient drift plasma instabilities (Type II irregularities) in the EEJ, forming the Esq layers (Resende et al. 2016; Rastogi 1972; Whitehead 1989).

Besides the well-established ground-based observations of sporadic E layers by ionosonde stations, the GNSS (Global Navigation Satellite System) radio occultation (RO) technique can be exploited to get information about this phenomenon from space. The RO method uses low Earth orbiting (LEO) satellites flying at a few hundred kilometer altitude to receive signals from the various GNSS constellations. The obtained profiles contain information on a broad spectrum of atmospheric and ionospheric parameters. A detailed description of the RO functional principle, its opportunities, and challenges are given by Hajj et al. (2002); Wickert et al. (2001); Kursinski et al. (1997).

In the ionosphere, RO profiles contain information on the electron density and also on irregularities forming here. GNSS amplitude or phase measurements show strong scintillations after passing, e.g., equatorial plasma bubbles in the ionospheric F region (Brahmanandam et al. 2012; Liu et al. 2016b; Kepkar et al. 2020) and sporadic E layers (Hocke et al. 2001; Wu 2006; Arras et al. 2008).

In this paper, we focus on the properties of sporadic E layers at low and equatorial latitudes. We will show their occurrence probability using comprehensive ground- and space-based data sets and discuss the difference between Esq and Esb layers. Chapter 2 introduces the data sets we are using in this study. Further, we will focus on the difference between Esq and Esb layers and demonstrate that the Esq is commonly not visible in radio occultation soundings. Chapter 3 presents satellite data-based sporadic occurrence rates (OR) and mean altitudes of the Es layers on the globe but focuses on the tropical region. We concentrate mainly on the longitudinal structure in both parameters. The succeeding discussion section explains possible reasons for the observed sporadic E properties close to the magnetic equator. We compare the results with equatorial electric field (EEF) measurements performed by the Swarm constellation. The summary in chapter 5 concludes the paper.

Analysis of radio occultation and ionosonde soundings at low latitudes

In the last two decades, the GNSS RO technique has evolved from a pioneering technique to a multilateral standard tool for probing the whole atmosphere and ionosphere. Since the launch of the CHAMP satellite in July 2000, there exists a continuously growing number of satellites carrying a GNSS RO receiver. In this study, we are using data obtained from nine different satellite missions gathered between January 2007 and December 2021. In total, we analyzed 13,252,866 RO profiles. The annual amount of available RO measurements is displayed in Fig. 1. The different colors stand for the individual satellite missions. This figure highlights that the data availability has increased distinctly since the COSMIC-2 mission has been operational.

By far, the largest number of profiles has been measured by the FormoSat-3/COSMIC and FormoSat-7/COSMIC-2 missions. Both missions consist of six individual satellites. The spacecrafts of the COSMIC-1 mission were launched in April 2006 flying in polar orbits with 72° inclination angle, and with a 30° longitudinal separation at ∼ 800 km altitude (Anthes et al. 2008). The mission ended in early 2020. The observed gradual reduction of FormoSat-3/COSMIC profiles since 2015 is due to the aging of the satellites. The follow-on mission FormoSat-7/COSMIC-2 was launched in June 2019. The satellites fly at an altitude of about 550 km in evenly spaced

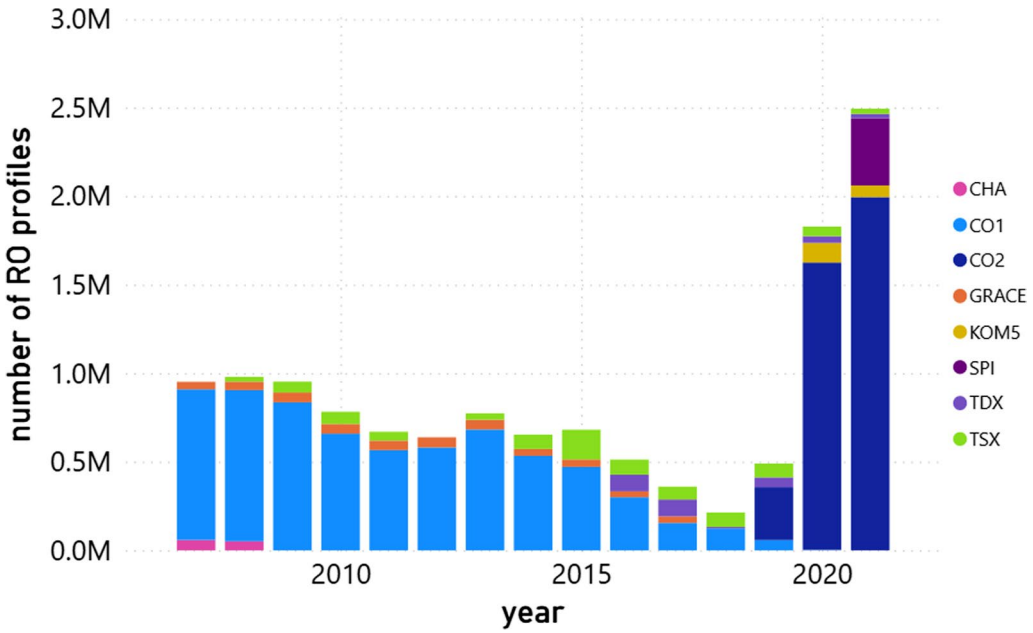

Fig. 1 Annual number of analyzed GNSS RO profiles. The different colors indicate the various satellite missions. The abbreviation CHA stands for the CHAMP satellite, SPI for Spire, KOM5 for KOMPSAT-5. CO1 and CO2 refer to the COSMIC missions and TDX and TSX stand for TANDEM-X, and TerraSAR-X, respectively

low inclined orbits of 24°. As a further development, the satellites are tracking GLONASS signals in addition to GPS (Schreiner et al. 2020). Additionally, we analyze measurements performed by the CHAMP and GRACE missions, that provided data until 2009 and 2017, respectively (Wickert et al. 2004; Ward et al. 2004). The spacecraft twins Tandem-X and TerraSAR-X orbit the Earth at around 515 km altitude in a helix formation. Their main purpose is to provide high-resolution SAR interferometry images of the Earth's surface (Krieger et al. 2007). Both satellites also carry a GPS occultation antenna and contribute to the RO database with 200 measurements per day since 2008 and 2016, respectively. We further include data from the South Korean Kompsat-5 satellite. This mission was launched in August 2013 with the main focus on acquiring independent high-resolution SAR (synthetic aperture radar) images (Choi et al. 2010; Lee et al. 2020). Additionally, the satellite has provided approximately 400 RO profiles per day since July 2019. From autumn 2021, RO measurements from satellites owned by the commercial company Spire are available and complete our data set since autumn 2021. Spire's cube-sat constellation currently provides about 4000 globally distributed RO profiles per day. The spacecraft are designed to receive signals from multiple GNSS constellations like GPS, Galileo and GLONASS (Masters et al. 2019; Bowler 2020).

This study uses the signal-to-noise (SNR) profiles of the GNSS L1 signal which is included in the level 1b atmPhs or conPhs data product. The profiles have a high sampling rate of usually 50 Hz, which refers to a height resolution of ∼ 50 m at the E-region. The recent FormoSat-7/COSMIC-2 mission provides a sampling rate of 100 Hz. This fact improves the height resolution even more to about 25 m at 100 km altitude. The SNR frequently experiences fluctuations at different altitude levels originating from vertical gradients of different parameters in the atmosphere and ionosphere (Hajj et al. 2002; Wu et al. 2005; Wu 2006). Since we are focussing on the lower ionosphere, we like to avoid any effects from the lower atmosphere. Therefore, we consider only the part between 70 km and the upper boundary of the profile that is usually located at a tangent height between 130 km and 140 km, except for Spire's data whose profiles sometimes cover even parts of the F-layer. The SNR free space value (SNR0) is almost constant above ∼ 35 km altitude and varies distinctly between the different satellite missions but also from occultation to occultation. In order to combine the datasets anyway, each profile is normalized by dividing the SNR values by the mean value of the respective profile between the upper boundary of the profile and 70 km altitude. At ionospheric altitudes, the SNR is very sensitive to sudden vertical changes in the electron density. Under undisturbed conditions and in absence of sharp gradients, the SNR varies slightly around the SNR0 (cf. Fig. 3). In case the signal propagates through a sporadic E layer, the SNR fluctuates strongly at this specific altitude range (see Fig. 2). This effect is explained by a focussing/defocussing of the GNSS signal while it passes strong electron density gradients (Wu et al. 2005; Hajj et al. 2002; Wickert et al. 2004).

For extracting sporadic E layer information from the profiles, we generally follow the method described by Arras and Wickert (2018). Therefore, we calculate the standard deviation in a 2.0 km altitude running window. If the standard deviation exceeds 0.2, we categorize the

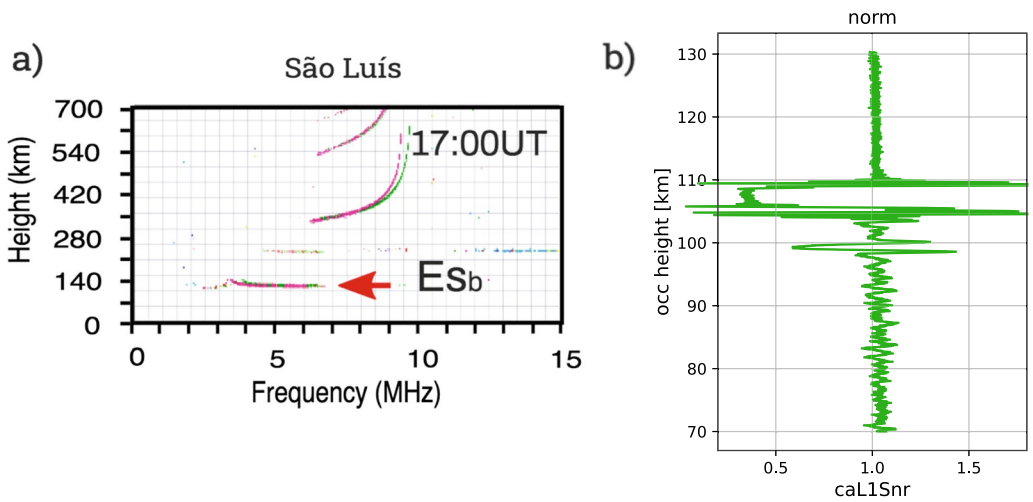

Fig. 2 **a** Ionogram of a strong sporadic E layer seen as an Esb at São Luís in the afternoon of 21 February 2021. Plot **b** shows a co-located (2.0°S, 43.5°W) normalized SNR profile including an intense Es signature. The RO sounding was recorded by COSMIC-2 satellite E2 at 17:05 UT

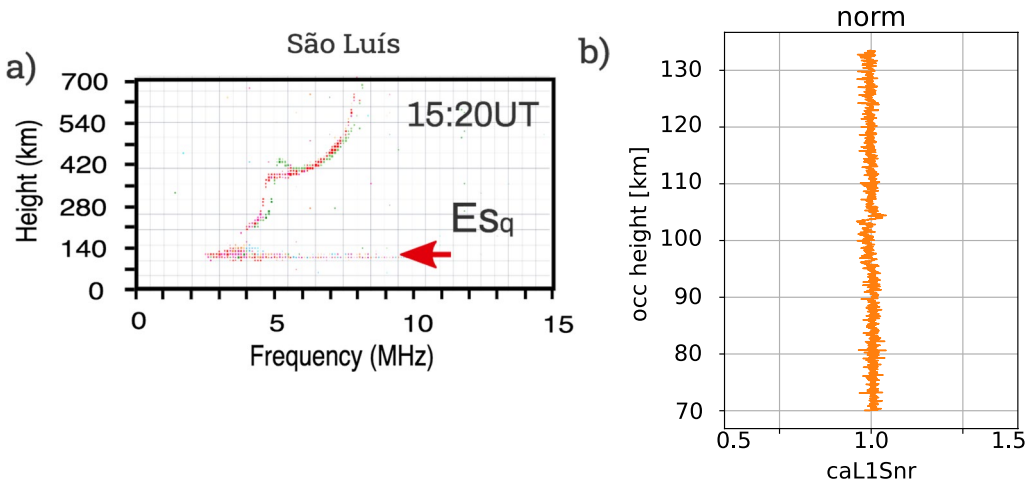

Fig. 3 Plot **a** shows an ionogram recorded by the São Luís station in the afternoon of 1 May 2006. The ionogram shows an Esq signature. Plot **b** illustrates a co-located (2.6°S, 42.5°W) normalized SNR profile recorded by the CHAMP satellite at 15:06 UT. The Esq layer is not visible in the SNR profile

single profile as disturbed. Further, the mean standard deviation of the whole profile should be lower than 0.11 in order to eliminate profiles showing high measurement noise. In the next step, we check the height range of large standard deviation values. Only if the disturbed part is concentrated within a 10 km segment, the profile is finally classified as a sporadic E profile. It is also possible to estimate the altitude of the sporadic E layer. The point where the SNR shows the strongest deviation from the SNR0 is considered as the Es height. With this technique, we detect the region of strongest electron density gradient usually slightly above or below the electron density maximum. Nevertheless, the Es altitudes from RO agree well but with a few kilometers offset from the virtual heights gained by ionosondes (Resende et al. 2018; Arras and Wickert 2018). Finally, we obtain information on location, altitude and time of occurrence for every sporadic E layer.

The global distribution of GNSS RO measurements is not uniform in time and space. Generally, more profiles are available at lower and midlatitudes than in the polar regions. The reason for the uneven data distribution is the viewing angle of the LEO spacecraft with respect to the orbits of the GNSS satellites (see Arras (2010)). In order to avoid any influence from the data coverage on our results, we calculate sporadic E OR by dividing the amount of Es events in a grid cell by the total amount of available measurements.

Ionosondes are the most frequently used technique to observe sporadic E layers. Ionosondes work basically like a radar sending out frequencies ranging from 1 to 20–30 MHz. The signals are reflected at ionospheric layers related to the electron density. Thus, one gets information on the electron density of the different layers and from the signals' propagation time their altitudes can be estimated. The resulting ionograms contain further information about Es properties. Typical sporadic E layers that are formed by the wind shear process are relatively strong and dense. These layers are called blanketing layers since they partially or totally block the reflection of radio waves from the upper layers. It is important to mention that the Esb layers occur at latitudes away from the magnetic equator around 100–140 km (Resende et al. 2017). A strong blanketing sporadic E layer was measured by the ionosonde located at São Luís (2.3°S, 44.2°W), Brazil, on 21 February 2021. The ionogram (Fig. 2a) reveals that the Es blanketing frequency exceeds 6 MHz which refers to a peak electron density of 5.2 * 10^5 electrons cm^{-3} and it occurs at a virtual altitude of 115 km. The values of electron density (Ne) were calculated using the expression based on the relationship of $Ne = 1.24 * 10^4 * fbEs^2$ in electrons/cm^3, where fbEs is given in MHz. The fbEs parameter is obtained where the frequency of the upper layer starts to be observed in the ionograms. The same Es layer was observed by a COSMIC-2 RO event which took place at 2.0°S, 43.5°W at 17:05 UT. The SNR profile is displayed in Fig. 2b. It shows a strong scintillation stretching between 105–110 km altitude.

However, the wind shear mechanism requires inclined magnetic field lines to form compact sporadic E layers. Shears in the neutral winds lead to an accumulation of ions in the height range of the convergence null. The electrons follow the ions along inclined magnetic field lines to maintain charge neutrality. Justifiably, the process is

ineffective at the magnetic equator, where the magnetic field lines are arranged horizontally, and sporadic E formation based on wind shears is not possible. Nevertheless, a diffuse and non-blanketing Es trace covering most of the frequency scale is observed in ionograms over the equatorial sites. These layers are known as Esq and are associated with the equatorial electrojet current plasma instabilities, mainly the gradient drift instability (Type II irregularities) (Forbes 1981; Dhanya et al. 2008; Resende et al. 2016). An example is shown in Fig. 3, where it is possible to observe a clear trace of the Esq layer. For the Esq layer, the fbEs refers to the minimum trace of the F region. One characteristic of an Esq layer is that the F region trace is completely visible in ionograms and does not become blocked by the lower sporadic E layer like it is the case in the presence of an Esb layer. A relatively low peak electron density further characterizes the Esq layer. In our example, the Esq layer reaches 1.6 * 10^5 electrons m^{-3} which is almost a factor of 4 lower than the usual Esb layer presented in Fig. 2. In contrast, the Esq signal is completely absent in the co-located RO profile (Fig. 3b). This profile was recorded by the CHAMP satellite at 2.6°S, 42.5°W on 1 May 2006 at 15:06 UT. The missing of the typical Es scintillation can be explained by the weak manifestation of the Esq layer in terms of electron density gradients since the SNR only shows intense fluctuations when passing regions of strong vertical gradients in the electron density. Additionally, we compared 714 coinciding events between available RO profiles and ionosonde recordings to the examples we present here. We selected 306 RO profiles that are closely located (maximum distance of 0.5° in latitude/longitude and 10 minutes in time) to the São Luís ionosonde station and 408 RO events close to the Jicamarca ionosonde station. Both sites are located in the vicinity of the magnetic equator. However, it has been slowly drifting away from the São Luís ionosonde in recent years (compare with Fig. 9), which also explains the miscellaneous sporadic E types observed there. We will explain the impact of the drifting magnetic equator on sporadic E layers in more detail in the Discussion chapter. In 77 cases, we observed an Esq pattern in the ionogram, but only in three coinciding cases did we find sporadic E-like fluctuations in the SNR of the RO recordings. We conclude that there is a high chance that GNSS RO soundings are not capable of detecting Esq traces appearing close to the magnetic equator. Their electron density gradients are simply too small to lead to visible effects in the SNR recordings. This explains the apparently contrary results from RO measurements which do not detect Es signatures along the magnetic equator while studies using ionosonde soundings frequently report on sporadic E signatures of the Esq-type.

Results

Global sporadic E occurrence and altitudes

Existing global sporadic E occurrence maps (Arras et al. 2008; Liu et al. 2016a; Tsai et al. 2018) revealed that Es could be observed most frequently at lower and mid-latitudes. After the launch of several RO missions in recent years, the Es phenomenon can be illustrated in an unprecedented high spatial resolution using a combined data set. The sporadic E occurrence rate map in Fig. 4 is based on about 13 million of RO profiles collected

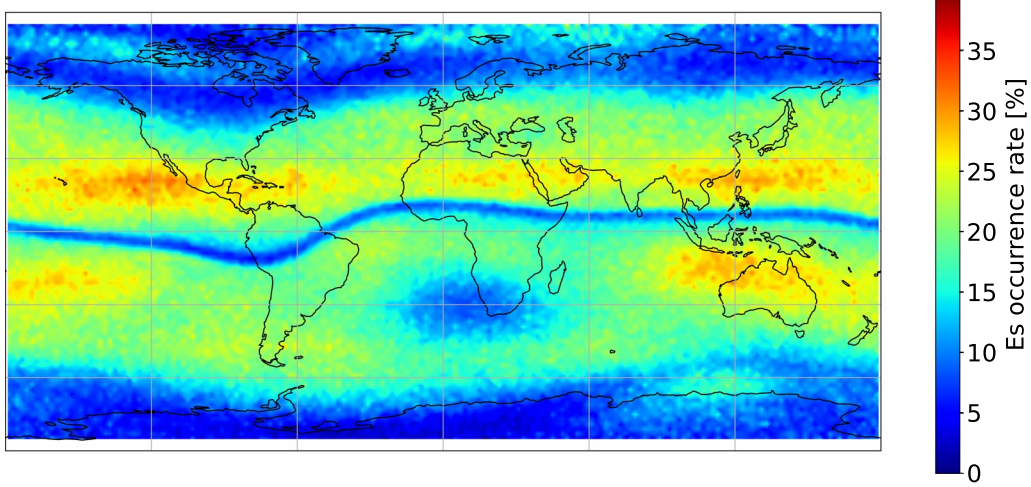

Fig. 4 Map of global sporadic E occurrence rate in a 2° x 2° resolution. This plot is a composite of RO data collected by several satellite missions between 2007 and 2021

between 2007 and 2021. The map reveals some interesting features. Obvious is the sharp and narrow belt of very low Es rates at low latitudes that follow exactly the course of Earth's magnetic equator.The vertical gradient of the zonal wind and the constant zonal wind in transition regions as Sao Luís, when we have the magnetic equator movement. Thus, the quantification of these parameters will be done in future works.The wind shear is not considered an effective mechanism to form the Es layer due to the impossibility of the electrons movement in the vertical lines, and the neutrality is not possible. Further, one can notice a depression in the Es rate in the South African region and a wave-like structure in the northern hemisphere. This minimum coincides accurately with the low values of the horizontal intensity of Earth's magnetic field and also the waveform in the northern hemisphere is visible here (compare with IGRF-13, Alken et al. (2021)).

Fig. 5 presents sporadic E altitudes in a 5° x 5° latitude–longitude grid estimated from the same data set used in Fig. 4. As expected, Es layers concentrate mostly between 100 km and 105 km with slight variability. Remarkable is that, again, the equatorial region shows a deviating pattern. Here, Es layers are detected in the mean at lower altitudes compared to the mid-latitude region. In the Indian region, we find the lowest Es altitudes on the globe except for the polar region, which raises the question of its origin.

In the left plot of Fig. 6, the Es layer altitude drop is manifested once more. The orange line represents the mean Es altitude (gray bars stand for the Es OR) over the magnetic latitude in a 5° resolution. Both, Es layer OR and mean altitudes maximize at midlatitudes of the northern and southern hemispheres. Close to the equator and at the cusp and polar regions the altitudes of Es layers are much lower. Obviously, the Es altitudes are higher at latitudes where its formation process relies on the wind shear alone. The mean Es altitudes drop by several kilometers at regions where electric fields contribute or even

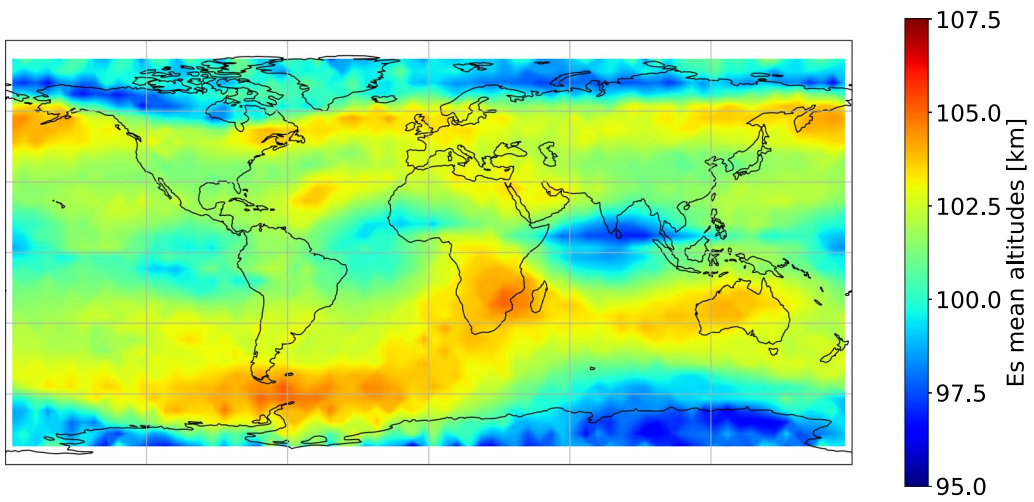

Fig. 5 Map of mean sporadic E altitude in a 5° x 5° resolution. This plot is a composite of RO data collected by several satellite missions between 2007 and 2021

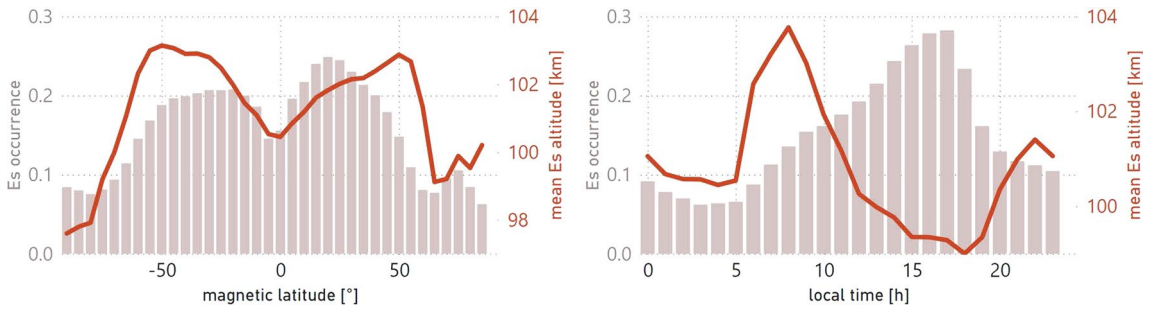

Fig. 6 Mean sporadic E occurrence and altitudes (2007–2021). The left plot shows the latitude dependent sporadic E occurrence (gray columns) and altitudes (orange line) in a 5° latitude resolution. The right plot reveals the local time-dependent mean Es OR and altitude in a 10° belt around the globe along the magnetic equator

prevent the sporadic E layer formation. The right plot of Fig. 6 presents the daily cycle of occurrence of blanketing sporadic E layers and their altitude in a belt +/− 5° around the dip equator. Es prevalence and altitudes seem to be anticorrelated. Most Es layers are observed in the later afternoon hours, but their mean altitude reached its daily minimum at exactly the same time. This sporadic E behavior can be explained by the combined action of diurnal tidal winds and electric fields and will be elucidated in more detail in the discussion section.

The seasonal variability of equatorial Es OR (gray bars) and altitudes (orange line) with respect to longitude is shown in Fig. 7. Both parameters do not show the same pattern. Concentrating on the Es altitudes, we noticed a weakly pronounced wave-3 signature during northern hemispheric winter conditions (upper left plot) that modifies over time into a wave-4 signal which is most pronounced during summer (lower left plot) and autumn (lower right plot). This result is in line with studies by Sobhkhiz-Miandehi et al. (2022); Jacobi et al. (2021), who demonstrated that the diurnal eastward propagating tide with wavenumber 3 (DE3), which is usually seen as a wave-4 pattern from satellite data, has the largest impact on Es formation at low latitudes.

Although there is high variability in the sporadic E altitudes throughout the seasons, we noticed that the minimum in the Indian sector is present during the whole year. As expected, this minimum coincides with the one visible in Fig. 5, which contains Es layer altitude information for the entire years 2007–2021.

Equatorial electric field data from Swarm measurements

The Swarm mission consists of three identical satellites launched in November 2013. The mission's main purpose is to observe the dynamics of Earth's magnetic field and to investigate the interactions with further geophysical and solar–terrestrial parameters (Olsen et al. 2013; Friis-Christensen et al. 2008). Satellites A and C are flying in almost identical near-polar orbits with an inclination of 87.4° at an altitude of about 450 km. The third of the Swarm satellites (Swarm B) flies at a higher elevation of ∼ 520 km with slightly different orbit parameters. As described by Alken et al. (2015), measurements from the Absolute Scalar Magnetometer instrument aboard the satellites can be used to determine the strength of the equatorial electrojet and the eastward component of the equatorial electric field (E_y) for every single satellite passing over the magnetic equator. The equatorial electrojet is a strong and narrow eastward flowing current that follows exactly the course of Earth's magnetic equator. It consists of a smaller Pedersen current and a superimposed stronger Hall current. The Pedersen current is driven by the eastward component of the EEF, which is generated by neutral tidal winds. The more intense Hall current is caused by a vertical polarization electric field

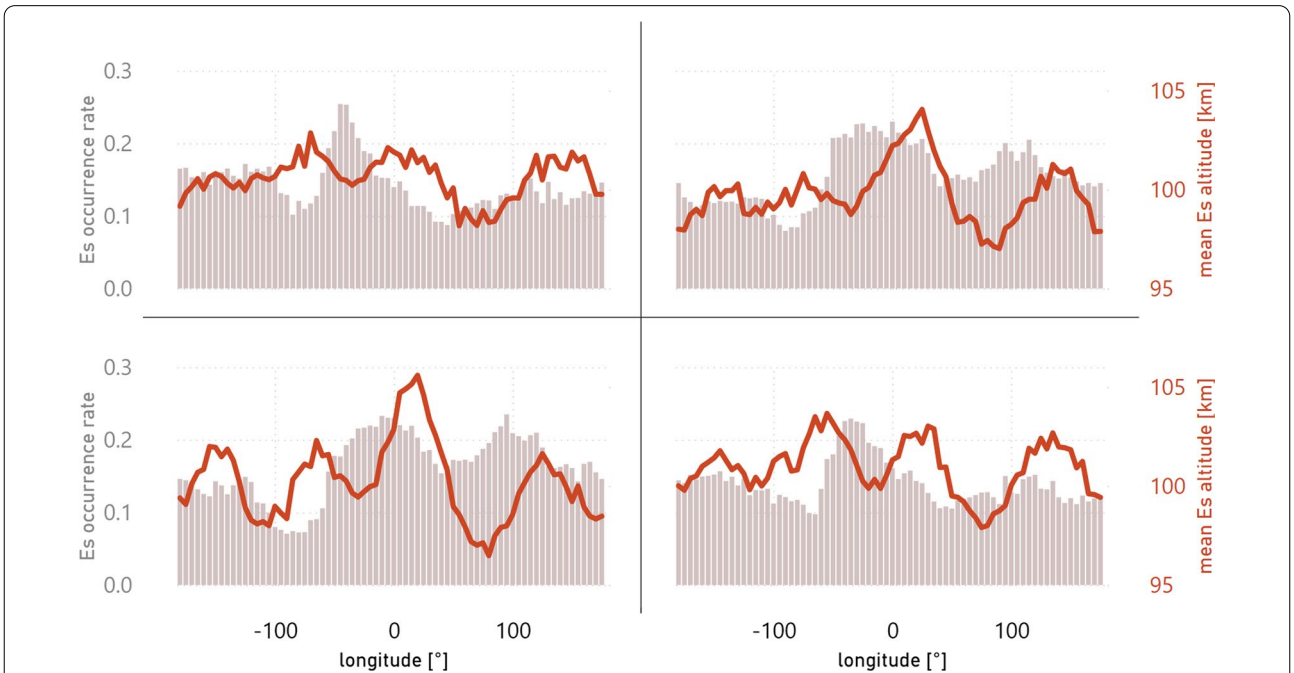

Fig. 7 Seasonal sporadic E occurrence rates (gray bars) and mean altitudes (orange line) along a narrow belt (+/−5°) following the magnetic equator. The upper row displays winter (left) and spring (right) conditions. Summer (left) and autumn (right) conditions are found in the bottom row

(E_z) (Forbes 1981; Moro et al. 2017,][and references therein).

The zonal EEF component, E_y, and its daily and seasonal variability are shown in Fig. 8. The data are taken from the Level 2 EEF data product provided by the Swarm A and C satellites. We calculated seasonal means of the zonal EEF component in a 10° longitude and 1 h local time grid for the period between 2014 and 2021. The resulting figures show the well-known features of an eastward directed E_y component during daytime. However, there is strong daily, seasonal, and also longitudinal variability. Generally, strong E_y values are observed in the Indian region between 60°E and 110°E, while relatively low values are found in a sector between 30°W and 80°W. Moro et al. (2017); Resende et al. (2016) investigated the response of sporadic E layers to electric fields in the equatorial region. The authors presented two facts that are valuable for our study presented here:

1) The zonal E_y component is directly correlated with the E_z component of the EEF, the latter being stronger by about a factor of 10.
2) During geomagnetic quiet times, high values of the E_z component prevent ion convergence. Therefore, the formation of blanketing sporadic E layers becomes not possible.

Discussion

We can observe the different types of sporadic E layers at the São Luís ionosonde station because of the relatively fast temporal displacement of the Earth's magnetic equator in that region. For example, the ionosonde was located at − 1.9°S magnetic latitude in 2000 and at − 7.8°S in 2015. In other words, when São Luís was located close to the magnetic equator, we frequently observed the Esq layers in the ionograms since the EEF largely influences this region. In recent years, the influence of the EEF on plasma drift has reduced significantly here, and neutral winds control the plasma drift increasingly. As a result, Esb layers appear more frequently, and the amount of Esq layers gradually reduces. Yizengaw (2020) used magnetometer measurement aboard different LEO missions and found the displacement rate to be largest in the Brazilian region, with about 0.2° per year between 2000 and 2019. Several papers revealed the ionospheric response to the secular changes in the geomagnetic field (Abdu et al. 1996; Resende et al. 2013). In

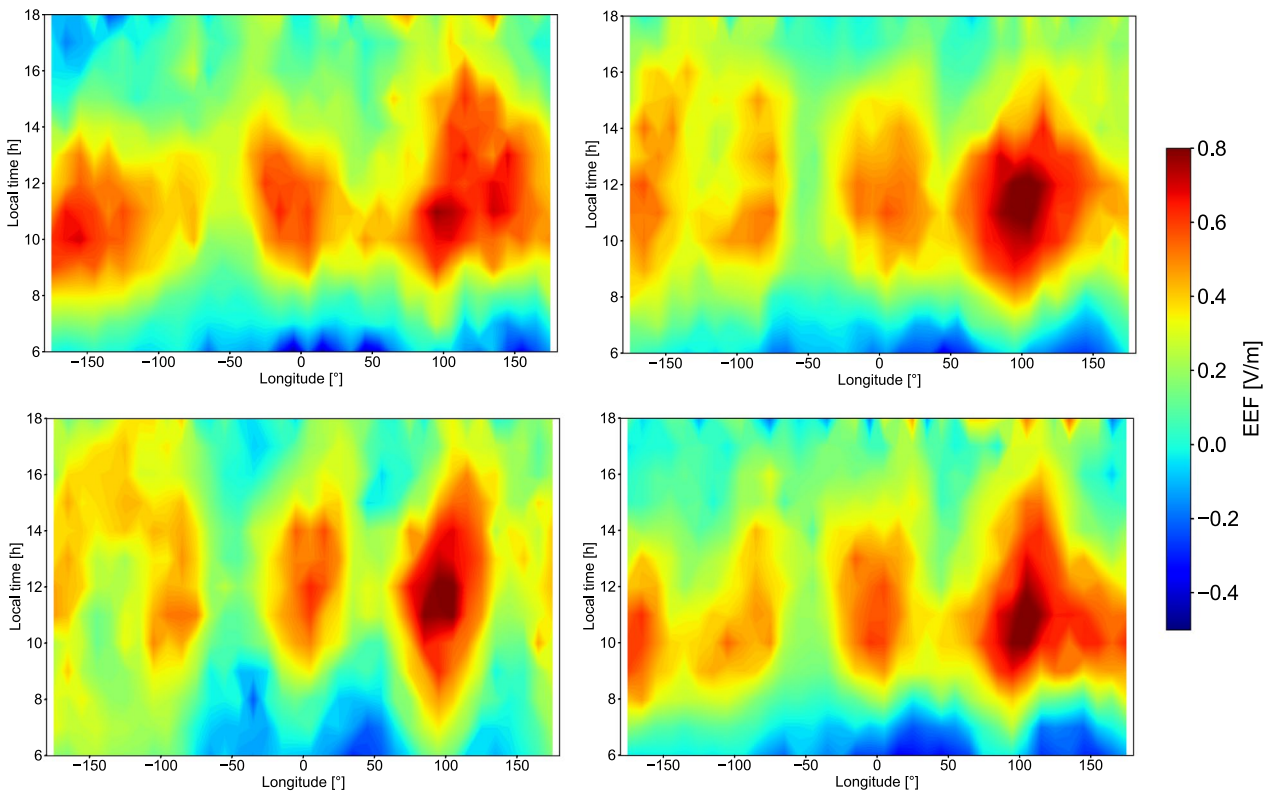

Fig. 8 Seasonal plots of the daytime eastward EEF as measured by the Swarm A and C satellites between 2014 and 2021. The plots in the upper row refer to the winter (left) and spring (right) seasons. The plots in the lower row represent summer (left) and autumn (right) conditions

Fig. 9, we present the sporadic E layer occurrence rates as measured by the RO technique in the South American Region between 2007 and 2021. A white line gives the position of the magnetic equator, and the location of the São Luís ionosonde is indicated as a red circle. In 2007, the magnetic equator was located close to the São Luís ionosonde station (− 5.2°S magnetic latitude), but it drifted away by several degrees in the following years. In 2021, the magnetic latitude there was given with − 11.4° S.

The sporadic E layer OR is very low in a narrow belt following exactly the course of the magnetic equator. Interestingly, one can also see the gradual drift of the magnetic equator in the position of the Es OR minimum region, which leads to the conclusion that the effect causing the minimum is also exclusively concentrated in a region of a few degrees around the magnetic equator. Further, we rarely observe sporadic E layers from RO measurements but at a relatively low altitude compared to midlatitudes. In the following, we propose an explanation for our observations. As discussed in chapter 2, these figures prove that GNSS RO can only identify Es formed by the wind shear process but not the gradient drift instability inside the electrojet that causes the Esq signatures in ionograms. However, vertical shears of the neutral wind do not describe the Es formation alone at equatorial latitudes. Electric fields have to be considered as well to describe ion accumulation. The following formula (1) defines the vertical ion velocity (V_{iz}) as a function of neutral winds and electric fields:

$$V_{iz} = \frac{\omega_i^2}{\nu_{in}^2 + \omega_i^2}\left[\cos(I)\sin(I)U_x + \frac{\nu_{in}}{\omega_i}\cos(I)U_y + \frac{1}{\nu_{in}}\frac{e}{m_i}\cos(I)\sin(I)E_x + \frac{e}{\omega_i m_i}\cos(I)E_y + \frac{e}{\nu_{in} m_i}\left(\frac{\nu_{in}^2}{\omega_i^2} + \sin^2(I)\right)E_z\right], \quad (1)$$

where ω_i is the ion gyrofrequency, ν_{in} is the ion-neutral collision frequency, I stands for the magnetic inclination, e represents the ion charge, m_i its mass, and U_x and U_y for the winds in meridional (southward) and zonal (eastward) direction. The electric field components are represented by E_x, E_y, E_z, where E_z stands for the upward pointing direction.

For convenient Es formation conditions, the vertical ion velocity has to be small, but its altitude derivation should be large. Since the $\sin(I)$ value is very low close to the equator, we can neglect all terms with the $\sin(I)$. Consequently, we only have to consider the zonal wind term and the zonal and vertical electric field. Both electric field components are of considerable magnitude directly at the altitude where the electrojet is flowing. Below, at the

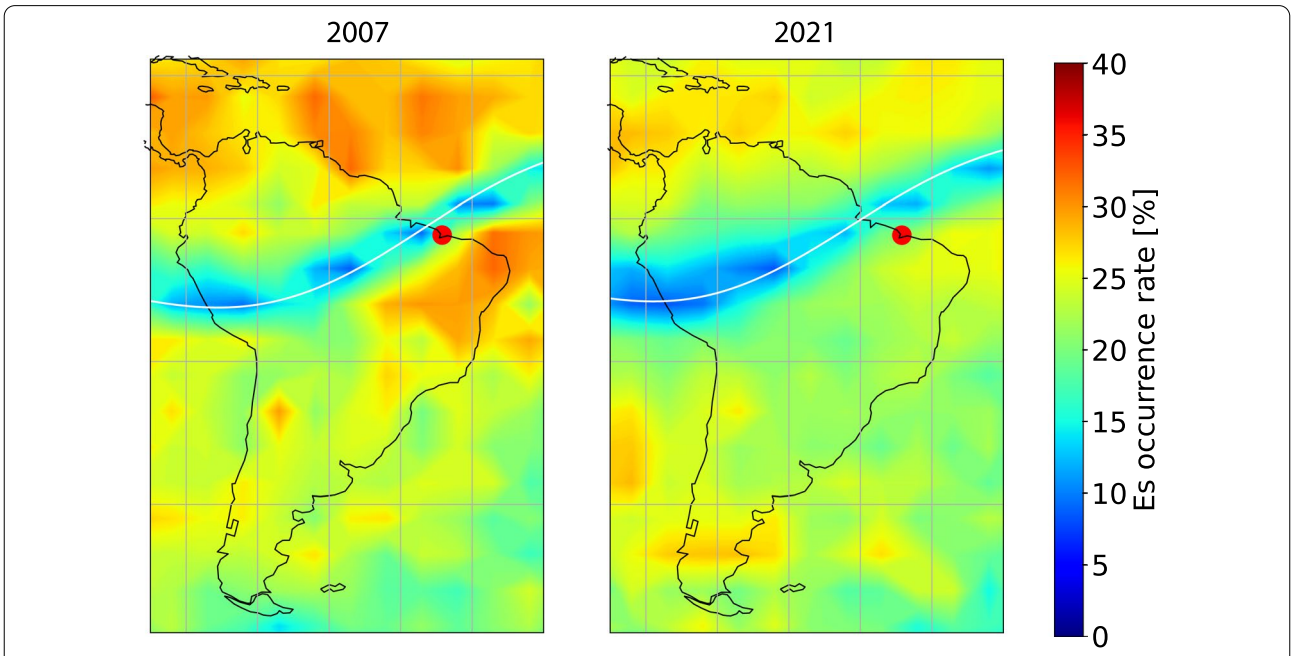

Fig. 9 Sporadic E occurrence rates in the South American region in 2007 (left) and 2021 (right). The São Luís ionosonde station is marked with a red circle. The position of the magnetic equator is given as a white line

height of around 90–100 km, the terms with electric field components can be ignored as well. Thus, Es layer formation depends only on the zonal wind. As a consequence, we would expect two different modes in the equatorial Es parameters over local time, an upper one that is influenced by the electric field and a lower one that is mostly driven by neutral wind.

In Fig. 10, we plotted the altitude-dependent equatorial sporadic E occurrence rate over local time. Therefore, we used RO data located in a band of 5°N/S around the magnetic equator. The plots represent seasonal means of northern hemispheric autumn conditions, including September, October, November of the years 2007–2021. We choose the autumn conditions because the difference between the longitude sectors is the largest here. The general pattern is similar throughout the year.

The illustration in the first row shows the conditions using all longitudes. The lower ones represent regions of low values of the eastward EEF in 30°W − 80°W (left) and of high values of the eastward EEF (right), including data collected from 60°E to 110°E, respectively. In the upper plot, we can, as expected, identify two different modes of sporadic E layers. The upper one descends from 115 km in the morning to about 100 km in the evening. The lower one has its maximum at ∼ 93 km and is concentrated in the afternoon hours. This pattern changes when we focus on smaller longitude sectors. The lower left plot represents the conditions for relatively low eastward EEF intensity (compare with Fig. 8). Here, the Es OR of both Es layer modes is of similar magnitude. The lower right plot shows the Es layer behavior in a region of high values of the eastward EEF, and sporadic E layers almost vanish above 100 km altitude. The lower mode is still present. Therefore, we conclude that both modes have a different origin.

As shown by simulation studies (Moro et al. 2017; Resende et al. 2016) and explained by Abdu et al. (2003), sporadic E traces of the blanketing type in the vicinity of the magnetic equator are formed by steady zonal westward directed diurnal and semidiurnal tidal winds and not necessarily by vertical shears in the wind field. Their

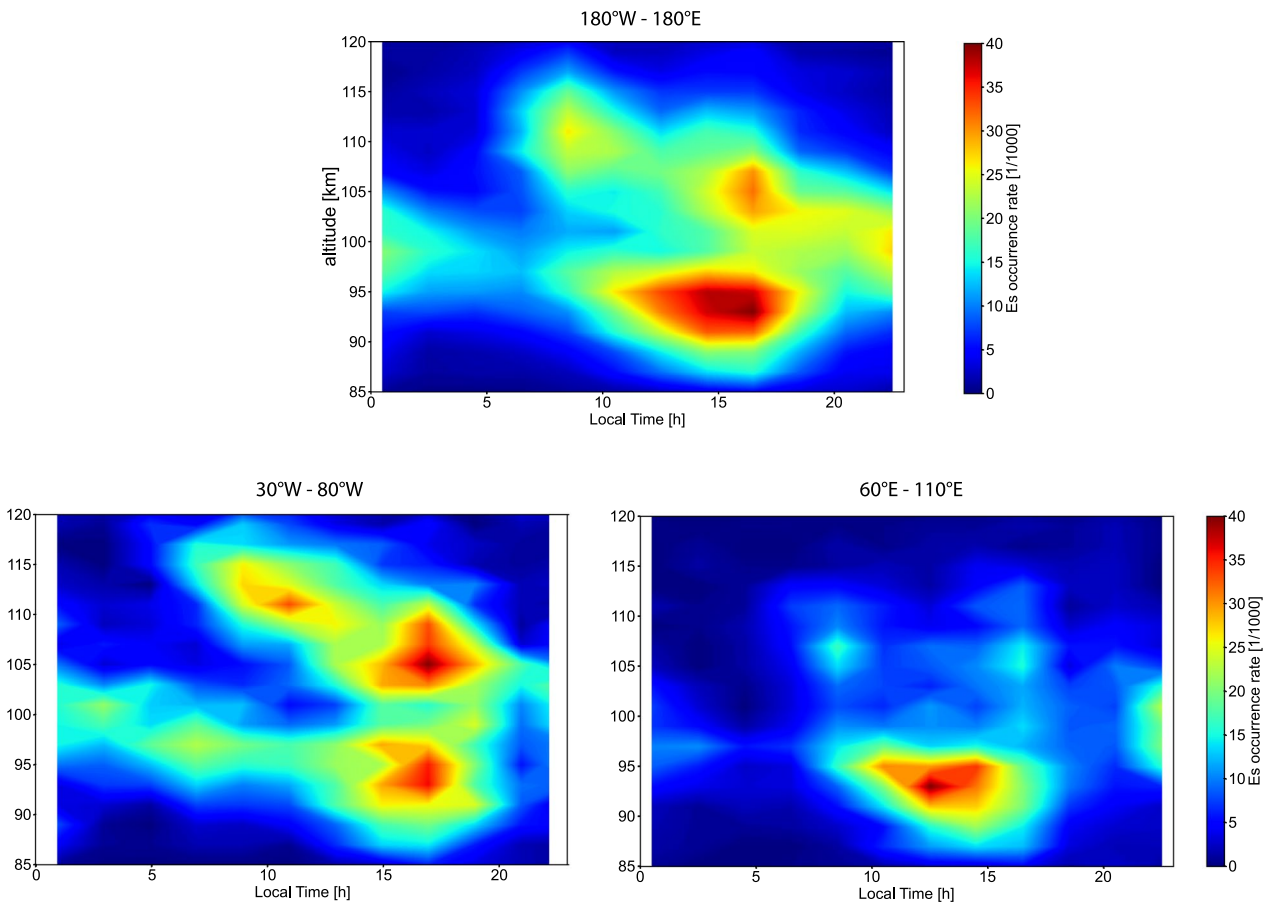

Fig. 10 Local time/altitude cross-sections of equatorial sporadic E occurrence rate in autumn (September, November, December) 2007–2021 in a 1 h x 1 km altitude resolution at different longitude sectors

simulations also revealed that the Esb traces are quickly disrupted by positive vertical electric fields.

Since there is a direct correlation between the eastward and the vertical electric field component, this fact would explain the very low values of Es OR at altitudes above 105 km in regions of strong eastward EEF. To prove this anticorrelation between Es altitudes and the eastward EEF, we plotted both parameters in Fig. 11 for autumn conditions. Again, we used RO data located in a band of 5°N/S around the magnetic equator. Figure 11a displays the Es OR depending on longitude and local time. We considered only Es layers appearing at altitudes higher than 105 km that represent the upper mode of Es layers (cf. Fig. 10). These Es layers are located at altitudes of the equatorial electrojet or above where the plasma drift is mainly controlled by the EEF. When visually comparing Fig. 11a) and the corresponding plot of the EEF (lower right illustration of Figure 8), one can notice that the plots show similar structures, although both parameters behave reversely. In both we find the wave-4 structure, but high values in the EEF correspond to low values in the Es OR. Figure 11b is very similar to a), but refers to Es layers at altitudes below 105 km. On a first glance one can see that it deviates distinctly from Fig. 11a) and also from the EEF pattern. Therefore, we conclude that Es layers from the lower mode are not strongly affected by the daytime eastward electric field. In Fig. 11c, d, we compared the connection between both parameters directly. The lower left plot c) contains the EEF and sporadic E heights over the longitude. In figure d), we plotted the mean sporadic E altitudes against the eastward EEF. A correlation coefficient of $R = -0.69$ was calculated, demonstrating the clear anticorrelation of both parameters.

Therefore, Es layer OR below ~ 100 km seems not to be strongly affected by the EEF. Here, the tidal winds dominate their formation (Abdu et al. 2003; Sobhkhiz-Miandehi et al. 2022). We believe that, although the wind shear is not effective around equatorial regions, a steady

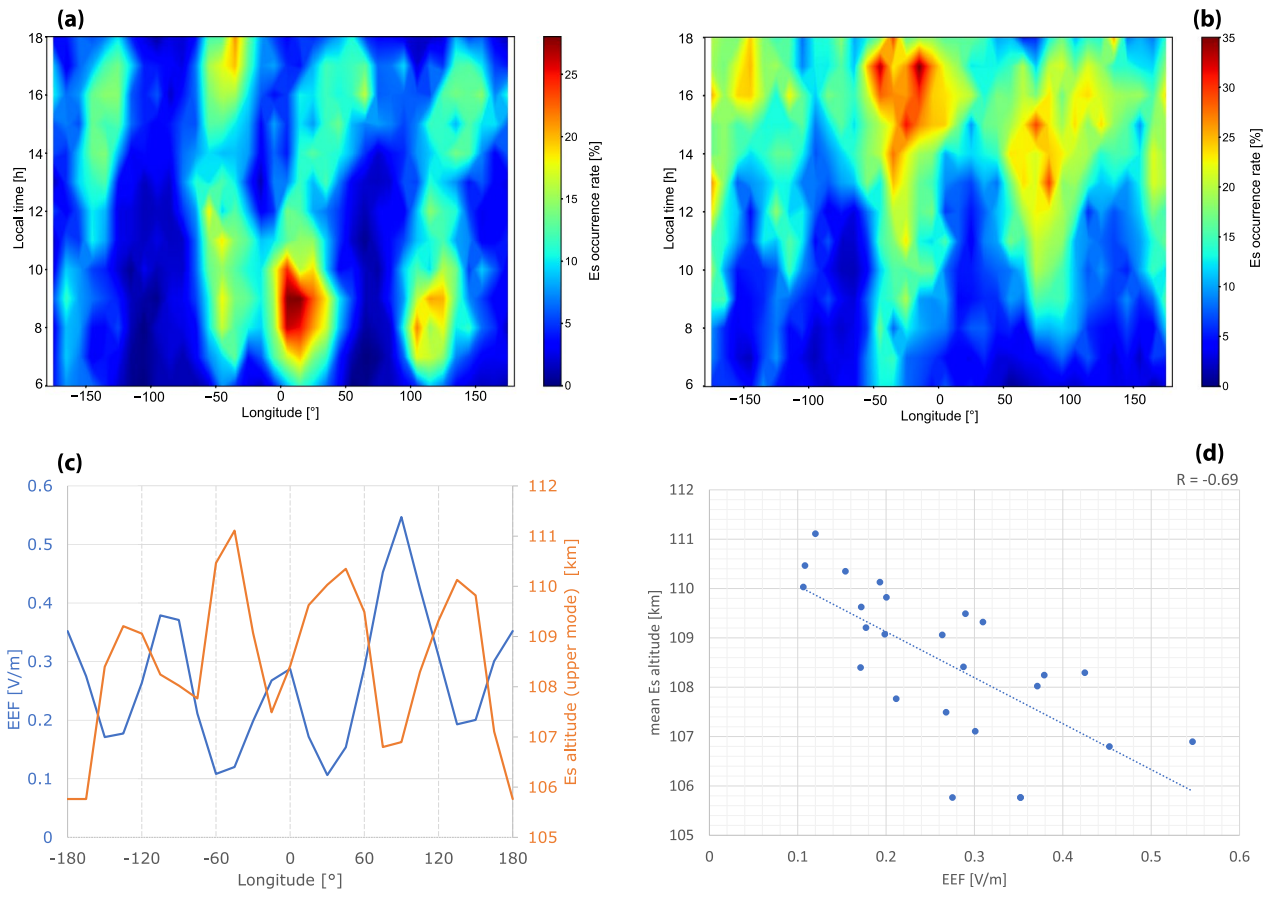

Fig. 11 **a** The plot shows the equatorial Es OR during autumn in a longitude–local time cross-section. For this plot, we considered Es events from the upper mode (altitude > 105 km). Image **b**: same as plot **a** but for Es layers appearing below 105 km. **c** Comparison of longitudinal variability of eastward EEF (blue) and the upper mode of equatorial sporadic E layers (orange). A clear anticorrelation ($R = -0.69$) of both parameters is observed and manifested in the lower right plot **d** where the Es altitude is mapped against the EEF

zonal westward directed wind can cause an ion convergence at altitudes below ~ 100km, as proposed by Abdu and Batista (1977). In fact, a negative gradient of the ion velocity (V_{iz}/dz of Equation 1) is capable of producing an electron density convergence in such a way that a sporadic E layer of the Esb type may be formed. Thus, the authors affirm that a steady zonal wind can create a negative vertical gradient in the vertical ion velocity, leading to the Es layer development. Also, this process can be effective because the electrons move in the horizontal component direction, and the plasma neutrality is sustained. Finally, our results show the first evidence of the tidal wind acting in equatorial and low altitudes (below 105 km) that form Es layers near the magnetic equator.

Summary

In this study, we have investigated sporadic E layer OR and heights in the equatorial region. Several satellite missions retrieved information about the sporadic E parameters from GNSS radio occultation measurements. We exploited SNR profiles of the GNSS L1 signal in order to identify strong scintillation effects at the altitude range between ~ 90 km to 130 km. Strong signal fluctuations in a narrow height range are attributed to sporadic E layers. These layers form due to the wind shear process preferably at low and midlatitudes. In the vicinity of the magnetic equator, the Esb layer is not formed by the wind shear process since it is not possible for the electrons to move in the vertical direction, and the neutrality is not maintained. Thus, a possibility for forming sporadic E layers of the blanketing type is that the strong eastward directed zonal wind leads to ion accumulation in horizontal direction. During daytime and at altitudes above approximately 100–105km, the equatorial eastward electric field interrupts the ion accumulation and the Es layers dissipate. Consequently, we observed altitude-dependent Es layer characteristics. At all altitudes, the Es formation is controlled by zonal winds. But at higher altitudes the eastward directed equatorial electric field leads to a dissipation of the accumulated ions. Both, Es layers and the EEF are affected by the zonal wind pattern which manifests in the appearance of the wave-4 structure. At this stage, we cannot judge exactly whether the EEF or directly the zonal wind has the largest impact on the zonal Es variability. This could be a topic for future research. Also to quantify the contribution of the zonal wind and its vertical gradient on the Esb layer formation at transition zones between equatorial and low latitude regions will be addressed in future works. Further, we could solve the existing contradiction that sporadic E layers are only rarely detected by GNSS RO soundings directly above the magnetic equator while ionosondes observe sporadic E layers of the q-type here. The Esq layers are attributed to the Type II irregularities inside the electrojet. They are more diffuse and not as compact as the blanketing type of the Es layer that is typically formed by wind shear.

Abbreviations

GNSS: Global Navigation Satellite System; RO: Radio occultation; Es: Sporadic E; OR: Occurrence rate; SNR: Signal-to-noise ratio; EEF: Equatorial electric field; EEJ: Equatorial electrojet; LEO: Low Earth orbit.

Acknowledgements

We thank the University Corporation for Atmospheric Research (UCAR) for providing the radio occultation data from several satellite missions. We also thank the European Space agency (ESA) for providing Swarm data. C. Arras acknowledges support by the DFG Priority Program DynamicEarth, SPP 1788 under grant AR953/1-2. L. C. A. Resende would like to thank the China–Brazil Joint Laboratory for Space Weather (CBJLSW), National Space Science Center (NSSC), Chinese Academy of Sciences (CAS) for supporting her postdoctoral. A. Kepkar was supported by DFG under grant SCHU1103/15-1.

Author contributions

CA designed the study, analyzed the RO and Swarm data, and wrote the paper. LR analyzed the ionosonde data, discussed the results and contributed to write the paper. AK and GS contributed to RO data analysis and discussion of the results. JW contributed to revise the paper. All authors read and approved the final manuscript.

Funding

Open Access funding enabled and organized by Projekt DEAL. C. Arras acknowledges the support by the DFG Priority Program DynamicEarth, SPP 1788 under grant AR953/1-2. L. C. A. Resende would like to thank the China–Brazil Joint Laboratory for Space Weather (CBJLSW), National Space Science Center (NSSC), Chinese Academy of Sciences (CAS) for supporting her postdoctoral. A. Kepkar was supported by DFG under grant SCHU1103/15-1.

Availability of data and materials

Radio occultation data are available under https://cdaac-www.cosmic.ucar.edu/. Data acquired by the Swarm constellation can be downloaded under https://swarm-diss.eo.esa.int/. Ionograms from the São Luís are accessible under https://www.digisonde.com/.

Declarations

Competing interests

The authors declare that they have no competing interests.

Author details

[1]GFZ German Research Centre for Geosciences, Potsdam, Germany. [2]State Key Laboratory of Space Weather, NSSC/CAS, Beijing, China. [3]National Institute for Space Research — INPE, São José dos Campos, Brazil. [4]TU Berlin, Berlin, Germany.

Received: 31 March 2022 Accepted: 10 October 2022
Published online: 07 November 2022

References

Abdu M, Batista IS (1977) Sporadic E-layer phenomena in the Brazilian geomagnetic anomaly: evidence for a regular particle ionization source. J Atmos Sol Terr Phys 39:723–731. https://doi.org/10.1016/0021-9169(77)90059-9

Abdu M, Batista I, Muralikrishna P, Sobral JA (1996) Long term trends in sporadic E layers and electric fields over Fortaleza, Brazil. Geophys Res Lett 23:757–760. https://doi.org/10.1029/96GL00589

Abdu M, MacDougall J, Batista I, Sobral J, Jayachandran P (2003) Equatorial evening prereversal electric field enhancement and sporadic E layer

disruption: a manifestation of E and F region coupling. J Geophys Res Space Phys. https://doi.org/10.1029/2002JA009285
Alken P, Maus S, Chulliat A, Vigneron P, Sirol O, Hulot G (2015) Swarm equatorial electric field chain: first results. Geophys Res Lett 42:673–680. https://doi.org/10.1002/2014GL062658
Alken P, Thebault E, Beggan CD, Amit H, Aubert J, Baerenzung J, Bondar T, Brown W, Califf S, Chambodut A, Chulliat A, Cox GA, Finlay CC, Fournier A, Gillet N, Grayver A, Hammer MD, Holschneider M, Huder L, Hulot G, Jager T, Kloss C, Korte M, Kuang W, Kuvshinov A, Langlais B, Leger J-M, Lesur V, Livermore PW, Lowes FJ, Macmillan S, Magnes W, Mandea M, Marsal S, Matzka J, Metman MC, Minami T, Morschhauser A, Mound JE, Nair M, Nakano S, Olsen N, Pavon-Carrasco FJ, Petrov VG, Ropp G, Rother M, Sabaka TJ, Sanchez S, Saturnino D, Schnepf NR, Shen X, Stolle C, Tangborn A, Toffner-Clausen L, Toh H, Torta JM, Varner J, Vervelidou F, Vigneron P, Wardinski I, Wicht J, Woods A, Yang Y, Zeren Z, Zhou B (2021) International geomagnetic reference field: the thirteenth generation. Earth Planets Space 73:1–25. https://doi.org/10.1186/s40623-020-01288-x
Anthes RA, Bernhardt PA, Chen Y, Cucurull L, Dymond KF, Ector S, Healy SB, Ho S-P, Hunt DC, Kuo Y-H, Liu H, Manning K, McCormick C, Meehan TK, Randel WJ, Rocken C, Schreiner WS, Sokolovskiy SV, Syndergaard S, Thompson DC, Trenberth KE, Wee T-K, Yen NL, Zhang Z (2008) THE COSMIC/FORMOSAT-3 mission: early results. Bull Am Met Soc 89(3):313–333. https://doi.org/10.1175/BAMS-89-3-313
Arras C (2010) A Global Survey of Sporadic E Layers based on GPS Radio Occultations by CHAMP, GRACE and FORMOSAT-3/COSMIC, STR 10/09, GFZ Potsdam, ISSN 1610-0956
Arras C, Wickert J (2018) Estimation of ionospheric sporadic E intensities from GPS radio occultation measurements. J Atmos Sol Terr Phys 171:60–63. https://doi.org/10.1016/j.jastp.2017.08.006
Arras C, Wickert J, Jacobi C, Heise S, Beyerle G, Schmidt T (2008) A global climatology of ionospheric irregularities derived from GPS radio occultation. Geophys Res Lett. https://doi.org/10.1029/2008GL034158
Axford WI (1963) The formation and vertical movement of dense ionized layers in the ionosphere. J Geophys Res 68:769
Bowler NE (2020) An assessment of GNSS radio occultation data produced by Spire. Q J R Meteorol Soc 146:3772–3788. https://doi.org/10.1002/qj.3872
Brahmanandam PS, Uma G, Liu JY, Chu YH, Latha Devi NSMP, Kakinami Y (2012) Global S4 index variations observed using FORMOSAT-3/COSMIC GPS RO technique during a solar minimum year. J Geophys Res Space Phys. https://doi.org/10.1029/2012JA017966
Choi M-S, Lee W-K, Cho S-K, Park J-U (2010) Operation of the radio occultation mission in KOMPSAT-5. J Astron Space Sci 27:345–352
Dhanya R, Gurubaran S, Emperumal K (2008) Lower E-region echoes over the magnetic equator as observed by the MF radar at Tirunelveli (8.7° N, 77.8° E) and their relationship to E sq and E sb, 26, 2459–2470, https://doi.org/10.5194/angeo-26-2459-2008
Forbes JM (1981) The equatorial electrojet. Rev Geophys 19:469–504. https://doi.org/10.1029/RG019i003p00469
Friis-Christensen E, Lühr H, Knudsen D, Haagmans R (2008) Swarm—an Earth observation mission investigating geospace. Adv Space Res 41:210–216. https://doi.org/10.1016/j.asr.2006.10.008
Hajj G, Kursinski E, Romans L, Bertiger W, Leroy S (2002) A technical description of atmospheric sounding by GPS occultations. J Atmos Sol Terr Phys 64:451–469
Haldoupis C (2010) A tutorial review on Sporadic E layers, Aeronomy of the Earth's Atmosphere and Ionosphere, IAGA Special Sopron Book series 2, Chapter 29, 381–394
Hocke K, Igarashi K, Nakamura M, Wilkinson P, Wu J, Pavelyev A, Wickert J (2001) Global sounding of sporadic E layers by the GPS/MET radio occultation experiment. J Atmos Sol Terr Phys 63:1973–1980
Jacobi C, Lilienthal F, Kandieva K, Yamazaki Y, Sobhkhiz-Miandehi S, Arras C (2021) Migrating and nonmigrating tidal signatures in sporadic E occurrence rates, Proceedings of Kleinheubach Conference, https://doi.org/10.23919/IEEECONF54431.2021.9598400
Jayachandran P, Sri Ram P, Rama Rao P, Somayajulu V (1999) Sequential sporadic-E layers at low latitudes in the Indian sector. Ann Geophys 17:519–525. https://doi.org/10.1007/s00585-999-0519-1
Kepkar A, Arras C, Wickert J, Schuh H, Alizadeh M, Tsai L-C (2020) Occurrence climatology of equatorial plasma bubbles derived using Formo-Sat-3/ COSMIC GPS radio occultation data, In: Annales Geophysicae, vol. 38, Copernicus GmbH, pp. 611–623. https://doi.org/10.5194/angeo-38-611-2020
Knecht R W and McDuffie R E (1962) On the Width of the Equatorial Es Belt, In: Ionospheric Sporadic, Pergamon Press, pp. 215–218. https://doi.org/10.1016/B978-0-08-009744-2.50022-9
Krieger G, Moreira A, Fiedler H, Hajnsek I, Werner M, Younis M, Zink M (2007) TanDEM-X: a satellite formation for high-resolution SAR interferometry. IEEE Trans Geosci Remote Sens 45:3317–3341
Kursinski ER, Hajj G, Hardy KR, Schofield JT, Linfield R (1997) Observing the Earth's atmosphere with radio occultation measurements using the Global Positioning System. J Geophys Res 102:23 429-465
Lee S-G, Lee S-J, Kim H, Chea T-B, Ryu D (2020) Status of the Kompsat-5 SAR Mission, Utilization and Future Plans, In: IGARSS 2020-2020 IEEE International Geoscience and Remote Sensing Symposium, IEEE, pp. 3552–3555
Liu J, Chen S, Yeh W, Tsai H, Rajesh P (2016) Worst-case GPS scintillations on the ground estimated from radio occultation observations of FORMOSAT-3/COSMIC during 2007–2014. Surv Geophys 37:791–809. https://doi.org/10.1007/s10712-015-9355-x
Liu JY, Chen SP, Yeh WH, Tsai HF, Rajesh PK (2016) Worst-case GPS scintillations on the ground estimated from radio occultation observations of FORMOSAT-3/COSMIC during 2007–2014. Surv Geophys 37:791–809. https://doi.org/10.1007/s10712-015-9355-x
Macleod MA (1966) Sporadic E theory. I. Collision-geomagnetic equilibrium. J Atmos Sci 23:96–109
Masters D, Irisov V, Nguyen V, Duly T, Nogués-Correig O, Tan L, Yuasa T, Ringer J, Sikarin R, Gorbunov M, Rocken C (2019) Status and plans for Spire's growing commercial constellation of GNSS science CubeSats, In: Proceeding of the Joint 6th ROM SAF User Workshop 7th IROWG Workshop, pp. 19–25
Mathews JD (1998) Sporadic E: current views and recent progress. J Atmos Sol Terr Phys 60:413–435. https://doi.org/10.1016/S1364-6826(97)00043-6
Moro J, Denardini CM, Resende LCA, Chen SS, Schuch NJ (2016) Equatorial E region electric fields at thedip equator: 1. Variabilities in easternBrazil and Peru. J Geophys Res Space Phys 121:220–230
Moro J, Resende L, Denardini C, Xu J, Batista I, Andrioli V, Carrasco A, Batista P, Schuch N (2017) Equatorial E region electric fields and sporadic E layer responses to the recovery phase of the November 2004 geomagnetic storm. J Geophys Res Space Phys 122:12–517. https://doi.org/10.1002/2017JA024734
Olsen N, Fris-Christensen E, Floberghagen R, Alken P, Beggan CD, Chulliat A, Doornbos E, Da Encarnacao JT, Hamilton B, Hulot G, van den Ijssel J, Kuvshinov A, Lesur V, Lühr H, Macmillan S, Maus S, Noja M, Olsen PEH, Park J, Plank G, Püthe C, Rauberg J, Ritter P, Rother M, Sabaka TJ, Schachtschneider R, Sirol O, Stolle C, Thébault E, Thomson AWP, Toffner-Clausen L, Velímský J, Vigneron P, Visser PN (2013) The Swarm satellite constellation application and research facility SCARF and Swarm data products. Earth Planets Space 65:1189–1200. https://doi.org/10.5047/eps.2013.07.001
Rastogi RG (1972) Equatorial sporadic E and plasma instabilities. Nat Phys Sci 237:73–75. https://doi.org/10.1038/physci237073b0
Resende L, Denardini C, Batista I (2013) Abnormal fb Es enhancements in equatorial Es layers during magnetic storms of solar cycle 23. J Atmos Sol Terr Phys 102:228–234. https://doi.org/10.1016/j.jastp.2013.05.020
Resende LC, Zhu Y, Denardini CM, Batista IS, Shi J, Moro J, Chen SS (2021) New findings of the sporadic E (Es) layer development around the magnetic equator during a high-speed solar (HSS) wind stream event. J Geophys Res Space Phys. https://doi.org/10.1029/2021JA029416
Resende LC, Arras C, Batista IS, Denardini CM, Bertollotto TO, Moro J (2018) Study of sporadic E layers based on GPS radio occultation measurements and digisonde data over the Brazilian region. Ann Geophys 36:587–593. https://doi.org/10.5194/angeo-36-587-2018
Resende LCA, Batista IS, Denardini CM, Carrasco AJ, de Fátima Andrioli V, Moro J, Batista PP, Chen SS (2016) Competition between winds and electric fields in the formation of blanketing sporadic E layers at equatorial regions. Earth Planets Space 68:1–14. https://doi.org/10.1186/s40623-016-0577-z
Resende LCA, Batista IS, Denardini CM, Batista PP, Carrasco AJ, de Fátima Andrioli V, Moro J (2017) Simulations of blanketing sporadic E-layer over the Brazilian sector driven by tidal winds. J Atmos Sol Terr Phys 154:104–114. https://doi.org/10.1016/j.jastp.2016.12.012
Schreiner WS, Weiss J, Anthes RA, Braun J, Chu V, Fong J, Hunt D, Kuo Y-H, Meehan T, Serafino W, Sjoberg J, Sokolovskiy S, Talaat E, Wee T, Zeng Z (2020)

COSMIC-2 radio occultation constellation: first results. Geophys Res Lett. https://doi.org/10.1029/2019GL086841
Shinagawa H, Miyoshi Y, Jin H, Fujiwara H (2017) Global distribution of neutral wind shear associated with sporadic E layers derived from GAIA. J Geophys Res Space Phys 122:4450–4465. https://doi.org/10.1002/2016JA023778
Sobhkhiz-Miandehi S, Yamazaki Y, Arras C, Miyoshi Y, Shinagawa H (2022) Comparison of the tidal signatures in sporadic E and vertical ion convergence rate, using FORMOSAT-3/COSMIC radio occultation observations and GAIA model. Earth Planets Space 74:88. https://doi.org/10.1186/s40623-022-01637-y
Tsai L-C, Su S-Y, Liu C-H, Schuh H, Wickert J, Alizadeh MM (2018) Global morphology of ionospheric sporadic E layer from the FormoSat-3/COSMIC GPS radio occultation experiment. GPS Solutions 22:1–12. https://doi.org/10.1007/s10291-018-0782-2
Ward A, Bagui M, Reigber C (2004) GRACE gravity recovery and climate experiment. Goddard Space Flight Center, Greenbelt
Whitehead J (1961) The formation of the sporadic-E layer in the temperate zones. J Atmos Terr Phys 20:49–58
Whitehead J (1989) Recent work on mid-latitude and equatorial sporadic-E. J Atmos Terr Phys 51:401–424
Wickert J, Reigber C, Beyerle G, König R, Marquardt C, Schmidt T, Grunwaldt L, Galas R, Meehan TK, Melbourne WG, Hocke K (2001) Atmosphere sounding by GPS radio occultation: first results from CHAMP. Geophys Res Lett 28(17):3263–3266
Wickert J, Pavelyev A, Liou Y, Schmidt T, Reigber C, Igarashi K, Pavelyev A, Matyugov S (2004) Amplitude variations in GPS signals as a possible indicator of ionospheric structures. Geophys Res Lett. https://doi.org/10.1029/2004GL020607
Wu DL (2006) Small-scale fluctuations and scintillations in high-resolution GPS/CHAMP SNR and phase data. J Atmos Sol Terr Phys 68:999–1017
Wu DL, Ao CO, Hajj GA, de la Torre Juarez M, Mannucci AJ (2005) Sporadic E morphology from GPS-CHAMP radio occultation. J Geophys Res. https://doi.org/10.1029/2004JA010701
Yamazaki Y, Arras C, Andoh S, Miyoshi Y, Shinagawa H, Harding BJ, Englert CR, Immel TJ, Sobhkhiz-Miandehi S, Stolle C (2022) Examining the wind shear theory of sporadic E with ICON/MIGHTI winds and COSMIC-2 radio occultation data. Geophys Res Lett. https://doi.org/10.1029/2021GL096202
Yizengaw E (2020) The potential impacts of the erratic motion of dip equator and magnetic poles. J Geophys Res Space Phys. https://doi.org/10.1029/2020JA028129

Publisher's Note